Proton Transfer Reactions on ^{26}Mg and ^{30}Si via the Reactions ^{26}Mg(^{3}He, d)^{27}Al and ^{30}Si(^{3}He, d)^{31}P†

H. F. Lutz, D. W. Heikkinen, W. Bartolini, and T. H. Curtis
Lawrence Radiation Laboratory, University of California, Livermore, California 94550
(Received 9 April 1970)

The proton transfer reactions on ^{26}Mg and ^{30}Si were studied using the reactions ^{26}Mg(^{3}He, d)^{27}Al and ^{30}Si(^{3}He, d)^{31}P at 17.85-MeV bombarding energy. Transitions to $T_>$ and $T_<$ levels were obtained. The spectroscopic factors from distorted-wave Born-approximation analysis were compared with information obtained at lower bombarding energies. The number of $T_<$ states is discussed qualitatively in terms of fragmentation caused by core-polarization states. The value for the isovector potential responsible for the splitting of the $T_>$ and $T_<$ states was determined for several orbits. Charge radii calculated for Coulomb energy differences indicated that ^{27}Al requires a larger radius parameter than ^{31}P.

INTRODUCTION

We have studied the proton transfer reactions ^{26}Mg(^{3}He, d)^{27}Al and ^{30}Si(^{3}He, d)^{31}P with a 17.85-MeV ^{3}He beam. The addition of a proton to a target with isospin T equal to its T_z component leads to states with $T_> = T + \frac{1}{2}$ and $T_< = T - \frac{1}{2}$ in the residual nucleus that has T_z equal to $T_<$. In the present experiment both targets have $T = 1$ and we produce states with $T_> = \frac{3}{2}$ and $T_< = \frac{1}{2}$ in the residual nuclei with $T_z = \frac{1}{2}$. The (p + target) states that have isospin $T_>$ are analogs of the low-lying levels in the (n + target) system, which can best be studied via the (d,p) reaction. The $T_>$ states are often high enough in excitation energy that they are unbound and therefore can be studied as resonances in the compound-nucleus system with proton scattering. In the present experiment we investigated states up to 10.50-MeV excitation in ^{27}Al and 9.40-MeV excitation in ^{31}P. The $T_<$ states, on the other hand, are usually bound and cannot be seen as resonances.

The targets in the present work were studied previously in separate experiments at lower bombarding energies. One purpose of the experiment was to compare the spectroscopic information derived at various bombarding energies. Bohne *et al.*[1] performed the ^{26}Mg(^{3}He, d)^{27}Al reaction at 11 MeV, and Alford *et al.*[2] studied the same reaction at 14 MeV. Our experiment looks at states higher in excitation than do those studies. The ^{30}Si(^{3}He, d)^{31}P reaction was studied at four angles by Betigeri *et al.*[3] with a 15-MeV ^{3}He beam. After the present work was completed, there appeared a high-resolution investigation of the ^{30}Si(^{3}He, d)^{31}P reaction at 12-MeV bombarding energy by Wolff and Leighton.[4]

The $J^\pi = \frac{1}{2}^+$, $T = \frac{3}{2}$ state at 6.815 MeV in ^{27}Al was first identified by Lawergren[5] in the reaction ^{26}Mg(d, n)^{27}Al using 3-MeV deuterons. States with $J^\pi = \frac{7}{2}^-$, $T = \frac{3}{2}$ at 10.48- and 10.51-MeV excitation were noted by van der Leun, Sheppard, and Endt[6] in their study of the ^{26}Mg(p,γ)^{27}Al reaction.

Davies, Dawson, and Neilson[7] analyzed the ^{30}Si(d, n)^{31}P reaction to identify the $J^\pi = \frac{3}{2}^+$, $T = \frac{3}{2}$ at 6.38 MeV and the $J^\pi = \frac{1}{2}^+$, $T = \frac{3}{2}$ at 7.15 MeV in ^{31}P. The $J^\pi = \frac{7}{2}^-$, $T = \frac{3}{2}$ level at 9.42 MeV was seen by Harris, Hennecke, and Prosser[8] using the ^{30}Si(p,γ)^{31}P reaction.

EXPERIMENTAL PROCEDURE

A beam of 17.85-MeV ^{3}He particles was momentum analyzed by a 90° bending magnet with a 76.2-cm radius of curvature, focused to a spot at the center of a 60.9-cm-diam scattering chamber. The beam was monitored by a Faraday cup and current digitizer.

The ^{26}Mg target was a self-supporting metallic foil with an areal density of 108 μg/cm^2. The ^{30}Si target was also self-supporting and had an areal density of 107 μg/cm^2. The isotopic enrichments were 99.77 and 95.20%.

The detector telescope used to observe the scattered particles subtended a solid angle of 2.50×10^{-4} sr. It consisted of a transmission-type surface-barrier ΔE detector and a lithium-drifted silicon E detector. The ΔE detector was 100 μm thick, operated with a reverse bias of 20 V, and the E detector was 2000 μm thick, operated with a reverse bias of 500 V. Both detectors were cooled by thermoelectric devices to −30°C to minimize leakage currents. The particle-identification circuit of Goulding *et al.*[9] was used to select deuterons from the reaction products. The spectra were stored in an 800-channel, pulse-height analyzer. The punched-paper-tape output of the pulse-height analyzer was used to generate computer cards that were used as input to the CDC-6600 computer. Computer programs were then used to plot the spectra, to fit the spectra with sums of Gaussian-

shaped peaks to obtain peak locations and areas, and to deduce and plot angular distributions. Data points were collected in $2\frac{1}{2}°$ steps starting at $12\frac{1}{2}°$.

The resolution of the present experiment was about 70 keV full width at half maximum. The energy groups are labeled where possible with the values listed in the compilation by Endt and van der Leun[10]; this is merely for convenience in comparing our results with other experiments, and is not intended as a claim of comparable accuracy.

EXPERIMENTAL RESULTS AND DWBA ANALYSIS

The angular distributions for the reactions ^{26}Mg-(^{3}He,d)^{27}Al and ^{30}Si(^{3}He,d)^{31}P are shown in Figs. 1, 2, and 3. The smooth curves in the figures are theoretical distorted-wave Born-approximation (DWBA) curves that were calculated using the computer code DWUCK written by Kunz.[11] The results of the DWBA analysis are summarized in Tables I and II. The computer code was run on a CDC-6600 computer at Livermore using the optical-model parameters given in Table III; these are the same parameters used by Bohne *et al.*[1] We also calculated with the ^{3}He parameters suggested by Zurmuhle and Fou[12] and the deuteron potential parameters used by Alford *et al.*[2] The results were not greatly affected by the various potentials.

The quality of the theoretical fits is in general quite good. In each reaction there were several transitions that could not be fitted or were too weakly excited to allow extraction of an angular distribution from the data. In ^{27}Al there are eight such levels, at 2209-, 4811-, 5550-, 5920-, 7050-, 8675-, 9670-, and 10 230-keV excitation energy. The 2209-keV level has $J^\pi=\frac{7}{2}^+$; we do not expect it

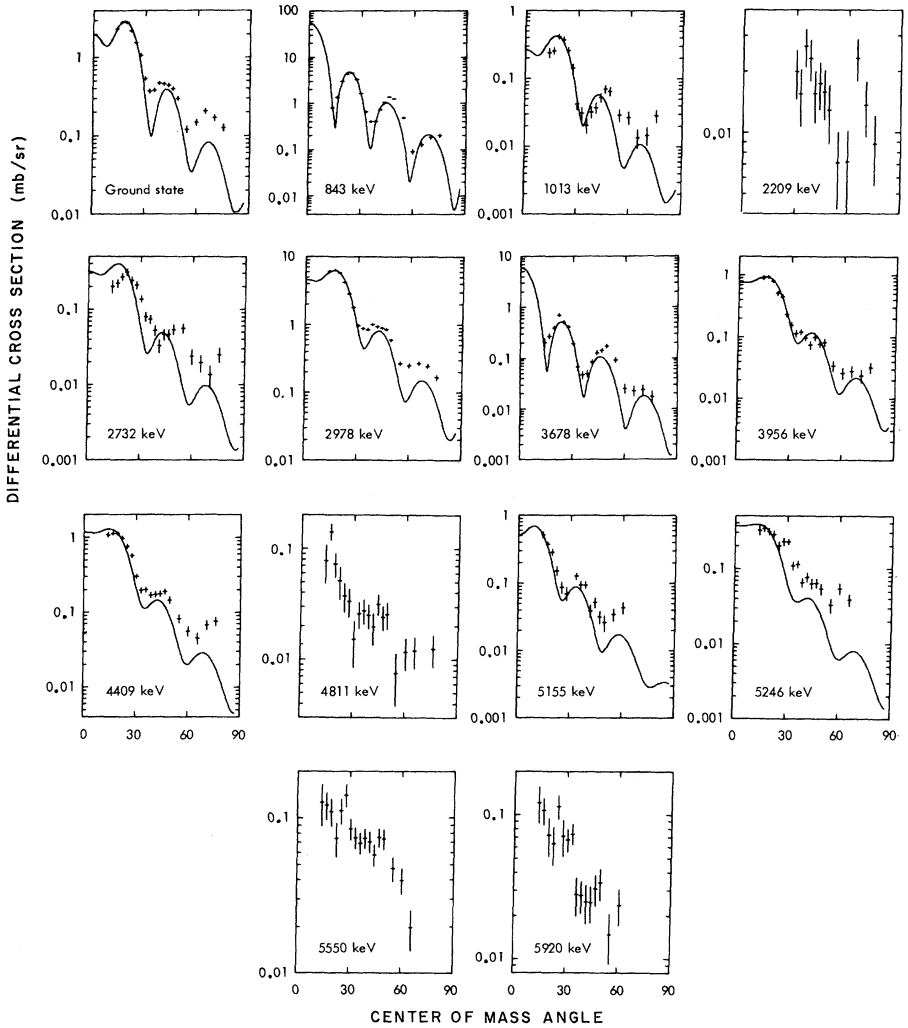

FIG. 1. Experimental angular distributions for 14 transitions for the reaction ^{26}Mg(^{3}He, d)^{27}Al. The solid curves are DWBA fits to the data. The spectroscopic information derived from the DWBA analysis is in Table I.

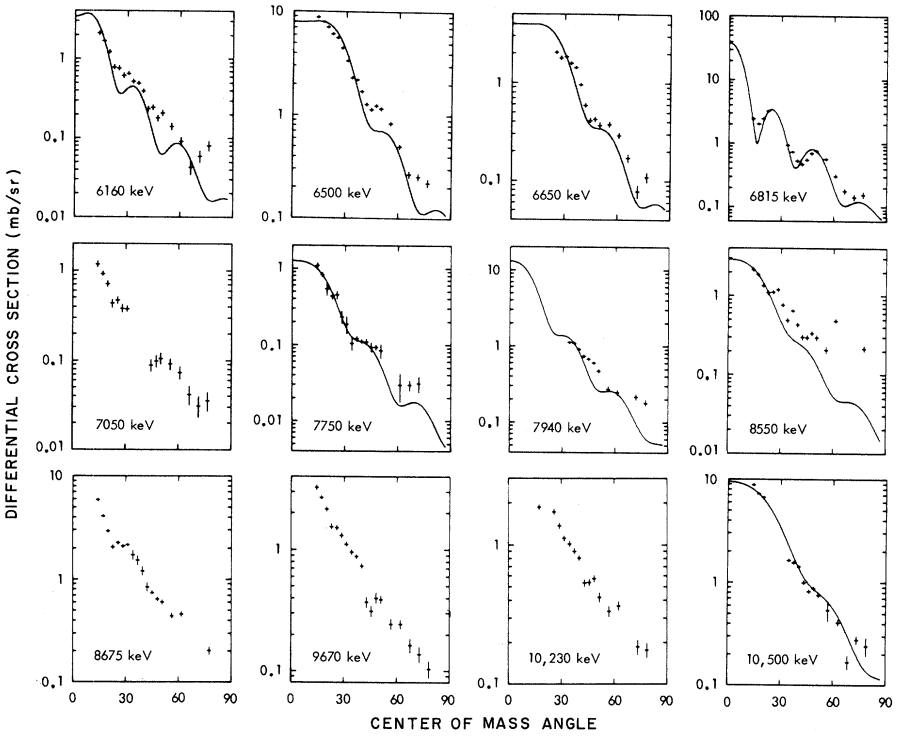

FIG. 2. Experimental angular distributions for 12 transitions for the reaction ^{26}Mg(^{3}He, d)^{27}Al. The solid curves are DWBA fits to the data. The spectroscopic information derived from the DWBA analysis is in Table I.

to be populated in a one-step process. The same situation occurs for the $\frac{9}{2}^+$ level at 3000 keV, which we do not see as a separate peak but which Alford *et al.*[2] have shown to be weakly excited. The 10 230 level is a doublet consisting of the $J^\pi = \frac{3}{2}^-$ state at 10 216 and the $\frac{1}{2}^+$ state at 10 240. In ^{31}P the levels at 3292, 3414, 3505, and 4188 keV were excited too weakly to extract angular distributions. The levels at 5590, 6240, and 7400 keV were not fitted with DWBA curves.

TABLE I. Summary of the results of the DWBA analysis for the reaction ^{26}Mg(^{3}He,d)^{27}Al. Details of the normalization procedure used for the spectroscopic factors are given in the text.

E_x (keV)	nlj	$(2J+1)C^2S$
g. s.	$1d_{5/2}$	1.5
843	$2s_{1/2}$	1.0
1013	$1d_{3/2}$	0.27
2732	$1d_{5/2}$	0.13
2978	$1d_{3/2}$	2.5
3678	$2s_{1/2}$	0.08
3956	$1d_{3/2}$	0.30
4409	$1d_{5/2}$	0.29
5155	$2p_{3/2}$	0.03
5246	$1d_{5/2}$	0.07
6160	$2p_{3/2}$	0.14
6500	$1f_{7/2}$	2.7
6650	$1f_{7/2}$	0.30
6815	$2s_{1/2}$	0.98
7750	$1d_{3/2}$	0.18
7940	$(2p_{3/2})$	0.55
8550	$(1d_{5/2})$	unbound
10 500	$1f_{7/2}$	unbound

TABLE II. Summary of the results of the DWBA analysis of the reaction ^{30}Si(^{3}He,d)^{31}P. Details of the normalization procedure used for the spectroscopic factors are given in the text.

E_x (keV)	nlj	$(2J+1)C^2S$
g. s.	$2s_{1/2}$	0.97
1266	$1d_{3/2}$	2.6
2234	$1d_{5/2}$	0.49
3135	$2s_{1/2}$	0.06
4260	$1d_{3/2}$	0.25
4431	$1f_{7/2}$	2.9
4592	$1d_{3/2}$	0.24
5015	$2p_{3/2}$	0.96
5254	$2s_{1/2}$	0.10
6380	$1d_{3/2}$	1.0
6520	$(2p_{3/2})$	0.29
6610	$(2p_{3/2})$	0.15
7150	$2s_{1/2}$	0.68
8190	$1d_{3/2}$	unbound
9404	$1f_{7/2}$	unbound

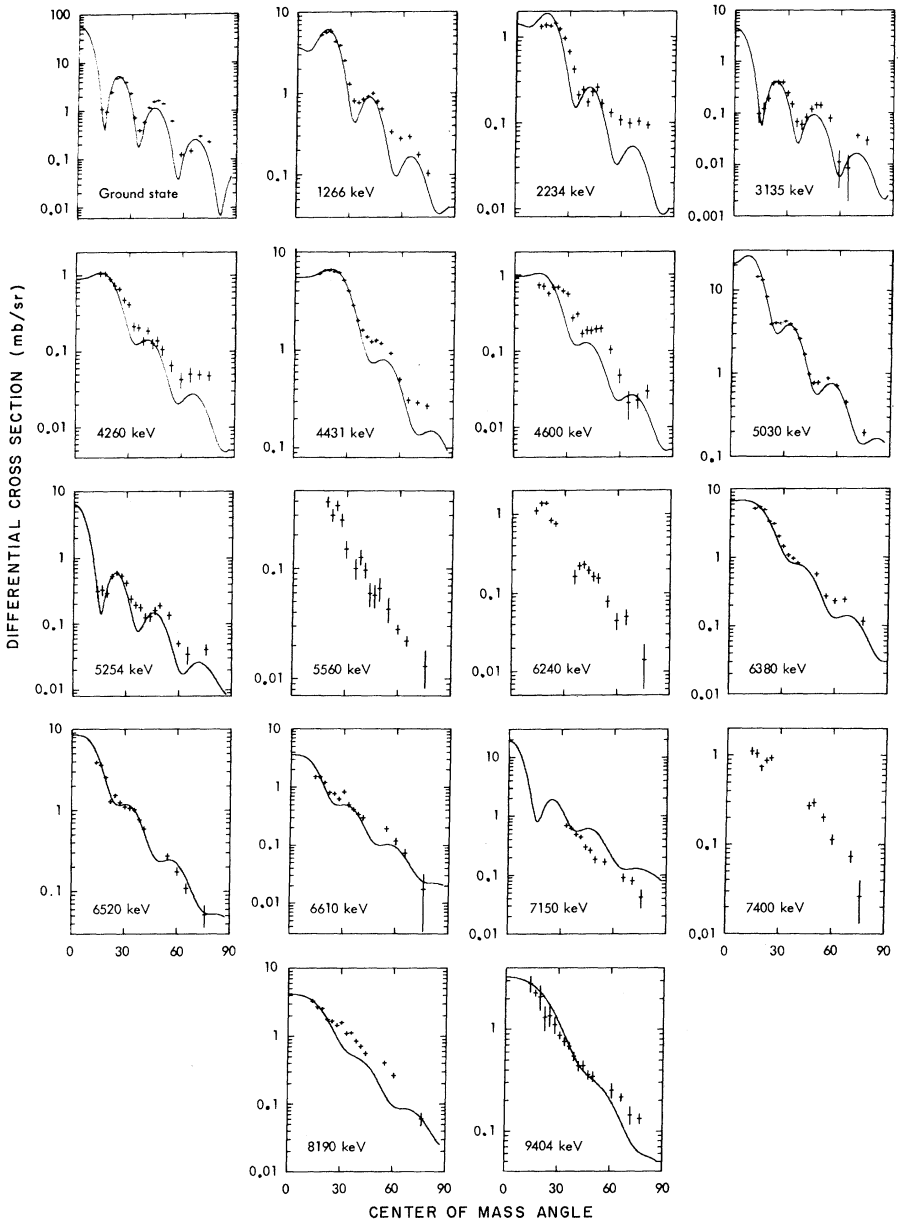

FIG. 3. Experimental angular distributions for 18 transitions for the reaction ^{30}Si(^{3}He, d)^{31}P. The solid curves are DWBA fits to the data. The spectroscopic information derived from the DWBA analysis is in Table II.

TABLE III. Optical-model parameters used in DWBA calculation.

Particle	V (MeV)	W (MeV)	W' (MeV)	V_{so} λ	r_0 (fm)	a (fm)	r_0' (fm)	a' (fm)	r_C (fm)	Nonlocality (fm)
^{3}He	155	15	•••	9.4	1.08	0.80	1.78	0.60	1.40	0.25
d	90	•••	22.5	12.	1.15	0.81	1.34	0.68	1.30	0.54
p	varied	•••	•••	25.	1.20	0.65	•••	•••	1.25	0.85

The spectroscopic information was extracted by matching the theoretical curve at some forward-angle maximum and using the relation

$$\left(\frac{d\sigma(\theta)}{d\Omega}\right)_{\text{exp}} = 4.42\, C^2 S_{1_{p_i},j}\, \sigma_{\text{DWUCK}}(\theta),$$

where $S_{1_{p_i},j}$ is the spectroscopic factor and C is the isospin Clebsch-Gordan coefficient. In our case $C^2 = \frac{2}{3}$ for proton transfers to $T_<$ states and $\frac{1}{3}$ for proton transfers to $T_>$ states. The $T_>$ levels are produced with the same spectroscopic factors as the analogous low-lying levels produced by (d,p) reactions on the same target, but the strength contains the factor $C^2 = \frac{1}{3}$. The factor 4.42 is a normalization factor for $(^3\text{He},d)$ reactions calculated by Bassel.[13] We further normalized our results to the sum rule, as will be explained below.

The sum rules given by French and Macfarlane[14] for proton-stripping strengths state:

$$G_p(T_>)_j = \frac{1}{2T+1}\langle \text{neutron holes}\rangle_j ,$$

$$G_p(T_<)_j = \langle \text{proton holes}\rangle_j - G_p(T_>)_j ,$$

$$G_p(T_>)_j + G_p(T_<)_j = \langle \text{proton holes}\rangle_j .$$

Using these relations and making the reasonable assumption that the positive-parity levels below the analog states represent the $T_<$ strength for the $1d_{5/2}$, $2s_{1/2}$, and $1d_{3/2}$ orbits, we have for ^{27}Al

$$\sum_j G_p(T_<)_j = 6$$

and for ^{31}P

$$\sum_j G_p(T_<)_j = \tfrac{14}{3} .$$

These sum-rule relations used to normalize the results of the DWBA analysis resulted in multiplying the ^{26}Mg$(^3\text{He},d)^{27}$Al results by 1.90 and the ^{30}Si-$(^3\text{He},d)^{31}$P results by 1.45. Our DWBA calculation used a finite-range correction of 0.77 and the nonlocality parameters listed in Table III. It contained no cutoff in the radial integrals. When Bassel applied the DWBA with the factor 4.42 to the reaction ^{48}Ca$(^3\text{He},d)^{49}$Sc (where one expects that $C^2S = 1$ for the ground-state transition), the local, zero-range calculation gave 0.92 whereas the nonlocal, finite-range calculation gave 0.66, requiring an additional correction of 1.5. Our correction factors of 1.90 for ^{27}Al and 1.45 for ^{31}P thus seem to be quite reasonable.

Where the transitions led to unbound levels, the DWBA code artificially set the binding at 20 keV and generated a curve that we used to compare with data, but it did not extract a value for the spectroscopic factor.

DISCUSSION

A. Comparison of Spectroscopic Information Obtained at Various Bombarding Energies

In Table IV we list the values for $(2J+1)C^2S$ for the transitions leading to the $T_<$ positive-parity levels of ^{27}Al. The 11-MeV data are those of Bohne *et al.*,[1] and the 14-MeV data are from Alford *et al.*[2] All the data are normalized to the sum rule as discussed previously. What we discuss here is how the strengths of these $T_<$ transitions are distributed. The agreement is generally satisfactory. There is a trend, as the bombarding energy increases, toward less strength in the ground state $J^\pi = \frac{5}{2}^+$ transition and more in the 2978-keV $J^\pi = \frac{3}{2}^+$ level, but this trend is not too strong, since the individual values vary from the mean by less than 20%.

The results for the transitions leading to $T_<$ positive-parity levels in ^{31}P are given in Table V. The 15-MeV data are due to Betigeri *et al.*[3] The 12-MeV data are those of Wolff and Leighton.[4] Again, the results are normalized by the sum rule; the comparison is satisfactory, although the run at the highest bombarding energy has less strength in the ground-state transition. It would be interesting to study these reactions at much higher bombarding energies to see if these trends persist.

B. Fragmenting of the $T_<$ States

It is informative to inspect the pictorial representation of some states in ^{27}Al and ^{31}P in n-p formalism corresponding to the expansions[15]

$$\chi_> = (2T_0+1)^{-1/2}[\chi_{pC} + (2T_0)^{1/2}\chi_{nA}]$$

and

$$\chi_< = (2T_0+1)^{-1/2}[\,(2T_0)^{1/2}\chi_{pC} - \chi_{nA}] .$$

TABLE IV. Distribution of $G_p(T_<)$ for the reaction ^{26}Mg$(^3\text{He},d)^{27}$Al leading to positive-parity levels in ^{27}Al.

E_x	J^π	11 MeV $(2J+1)C^2S$	14 MeV $(2J+1)C^2S$	17.85 MeV $(2J+1)C^2S$
g. s.	$5/2^+$	2.0	1.9	1.5
843	$1/2^+$	1.0	0.8	1.0
1013	$3/2^+$	0.3	0.3	0.3
2731	$5/2^+$	0.1	0.1	0.1
2978	$3/2^+$	2.1	2.1	2.5
3677	$1/2^+$	0.1	0.1	0.1
3956	$3/2^+$	0.2	0.3	0.3
4410	$5/2^+$	0.2	0.3	0.3

TABLE V. Distribution of $G_p(T_<)$ for the reaction ^{30}Si(^{3}He,d)^{31}P leading to positive-parity levels in ^{31}P.

E_x	J^π	12 MeV $(2J+1)C^2S$	15 MeV $(2J+1)C^2S$	17.85 MeV $(2J+1)C^2S$
g. s.	$1/2^+$	1.3	1.3	1.0
1265	$3/2^+$	2.7	2.6	2.6
2232	$5/2^+$	0.4	0.4	0.5
3133	$1/2^+$	<0.1	<0.1	<0.1
4257	$3/2^+$	<0.1	0.2	0.3
4592	$3/2^+$	0.1	0.1	0.2
5290	$1/2^+$	0.1	0.1	0.1

These are displayed in Figs. 4 and 5. The upper left diagram of each figure represents the $T=\frac{3}{2}$ states in the $T_z=\frac{3}{2}$ nucleus that are formed by adding a neutron to the core. These states are the parent states of the $T=\frac{3}{2}$ states in the $T_z=\frac{1}{2}$ nucleus, which are called the analog states (upper right diagram of each figure). In the diagram below each analog state are the $T=\frac{1}{2}$ states in the $T_z=\frac{1}{2}$ nucleus whose wave functions are orthogonal to the analog states. (These diagrams do not represent the structures of all the states we see in the proton transfer reactions studied in this paper. Specifically, they do not account for the $\frac{5}{2}^+$ states in the $A=27$ systems and the $\frac{1}{2}^+$ states in the $A=31$ systems. The core used in the diagrams implies that these states would not be seen in neutron-stripping and would have no $T_>$ strength in the proton-stripping reactions. Since this is not the case experimentally, the core must contain more complicated components such as two-particle–two-hole configurations.) In the $T_z=\frac{1}{2}$ part of the figure only the first term corresponding to $|pC\rangle$ carries the proton-stripping strength. The $|nA\rangle$ part of the configuration contains an n-p particle-hole pair with angular momentum $J_0=0$ and $T_0=1$. There may be another set of states, however, as indicated at the bottom of each figure; these, called core-polarization states, have $J_0\neq 0$ and do not carry any of the proton-stripping strength. These core-polarization states can admix with the antianalog state through the residual interactions and fragment the stripping strengths.[16] One can count the maximum number of core-polarization states by considering

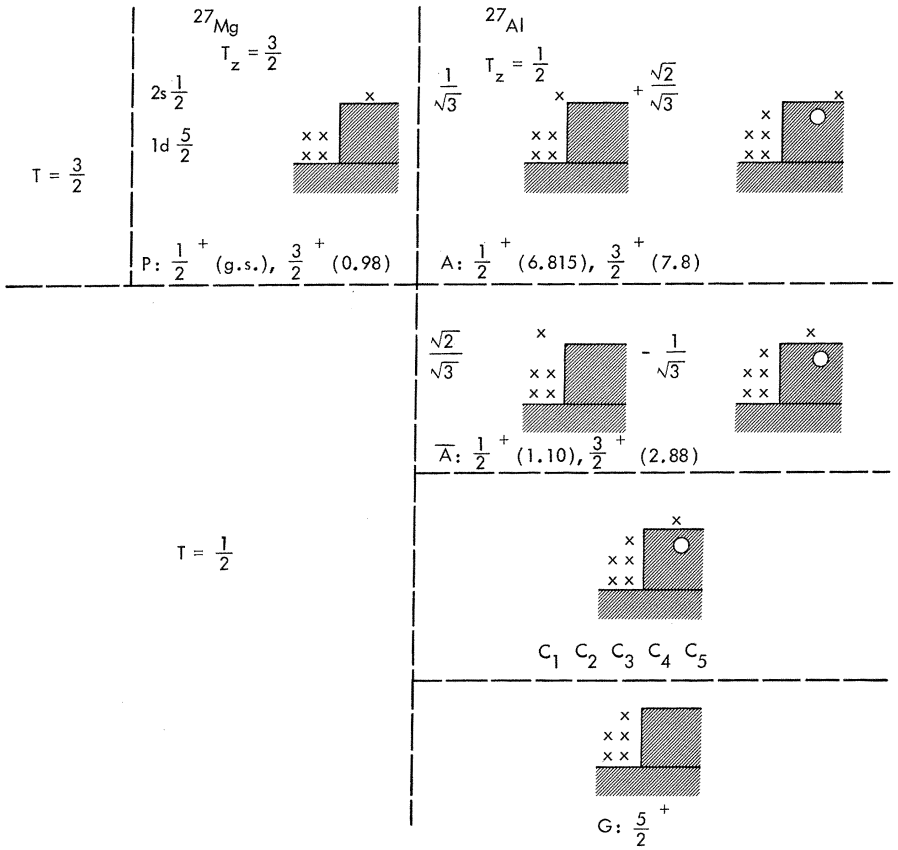

FIG. 4. Pictorial representation for the parent (P), analog (A), antianalog (Ā), and core-polarization (C) states using the simplest shell-model description for ^{27}Mg and ^{27}Al. The nuclear states are separated vertically by T_z and horizontally by T. The core structure is taken to be four protons in the $1d_{5/2}$ shell with a closed $1d_{5/2}$ shell for neutrons. G denotes ground state.

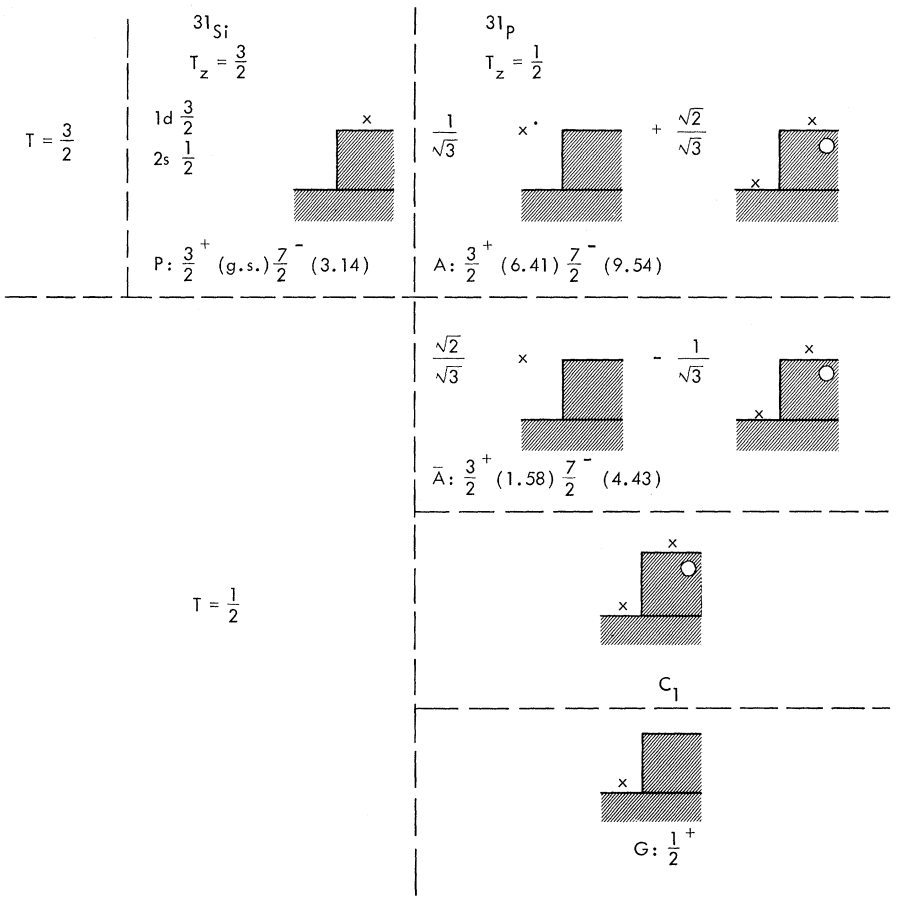

FIG. 5. Pictorial representation of some shell-model states in ^{31}Si and ^{31}P with a core closed to neutrons and empty of protons in the $2s_{1/2}$ shell.

the vector addition of the angular momenta involved. For ^{27}Al, for example, we have an n-p particle-hole pair in the $1d_{5/2}$ shell that can give $J=1, 2, 3, 4, 5$, and of these 1, 2, and 3 can vector-couple with $\frac{3}{2}$ to give $\frac{3}{2}$. There is only one core-excited state for $\frac{1}{2}^+$. This implies that there should be at most four $T_<$ states with $J^\pi=\frac{3}{2}^+$ and two with $J^\pi=\frac{1}{2}^+$; we see three and two, respectively.

In ^{31}P the n-p particle-hole pair is in the $2s_{1/2}$ shell and similar reasoning leads to one core-polarization state each for the $J^\pi=\frac{3}{2}^+$ and $\frac{7}{2}^-$ states. We should see at most two $\frac{3}{2}^+$ and two $\frac{7}{2}^-$ states. However, we see three and one, respectively. Consideration of more complicated diagrams for the $J^\pi=\frac{5}{2}^+$ states in ^{27}Al and $\frac{1}{2}^+$ states in ^{31}P lead to a maximum count of seven for the $\frac{5}{2}^+$ states and two for the $\frac{1}{2}^+$ states; we see three and two.

These considerations explain in a qualitative way why the spectrum of states seen in proton-stripping is less dense in ^{31}P than in ^{27}Al, but the extra $\frac{3}{2}^+$ state in ^{31}P requires more complicated wave functions.

C. Determination of the Isovector Potential

The positions of the analog states and the centroid of the $T_<$ states provide the information necessary to calculate the value of the potential V_1 appearing in Lane's coupled equations,[17] which is responsible for the splitting of the $T_>$ from the $T_<$ states. The difference in the depths of the potentials seen by these states is

$$V_> - V_< = (T_0 + \tfrac{1}{2})V_1/A\ ,$$

where T_0 and A are the isospin and mass of the target nucleus. This difference in potential depth is manifested in a symmetry energy ΔE_s given by the difference between the positions of the analog state and the centroid of the $T_<$ levels. As part of the DWBA calculation, the computer code calculates the depth of the central potential with a Woods-Saxon shape necessary to bind the proton with the correct binding energy. Inspection of these values for various transitions yields the variation of the potential depth with binding energy $\Delta V/\Delta B$ for each

shell-model orbit. The isovector potential is then given by

$$V_1 = \Delta E_s \frac{A}{T_0 + \frac{1}{2}} \frac{\Delta V}{\Delta B}.$$

The results of these calculations are summarized in Table VI. We have also included the data of Graue *et al.*[18] for ^{35}Cl reanalyzed in the manner described above. These authors studied the reaction ^{34}S(^{3}He,d)^{35}Cl, which is also a $T=1$ target proceeding to $T_> = \frac{3}{2}$ and $T_< = \frac{1}{2}$ states.

Vourvopoulos and Fox[19] studied the isospin splitting in ^{90}Zr and deduce a value of 148 MeV. In ^{55}Co the same type of analysis by Vourvopoulos, Fox, and Rosner[20] yields 113 MeV. Krasnov, Litvin, and Lyntin[21] calculated the behavior of the depth of the potential for neutron and proton single-particle states and deduced $V_1 = 170$ and 140 MeV, respectively. Their survey extended from Ca to Sn with values for V_1 varying from 90 to 250 MeV. The value for V_1 varies from 90 to 250 MeV. The value for V_1 from charge-exchange reactions was set at 109 MeV by Satchler, Drisko, and Bassel.[22] The value from proton elastic scattering was set by Sood[23] at 120 MeV. There is a clear tendency for the values of the isospin potential deduced from bound-state analyses to be greater than those from continuum analyses. This is possibly an indication of the energy-dependence of the isovector potential.

D. Coulomb Energy Differences and Charge Radii for Analog States

The Coulomb energy differences for the ground-state and excited-state analogs are shown in Table VII for ^{27}Mg–^{27}Al and in Table VIII for ^{31}Si–^{31}P. The values for ΔE_C were calculated using

$$\Delta E_C = E_x - Q[\text{parent } (p,n)],$$

TABLE VI. Values of isovector potential deduced from splitting of the $T_>$ and centroid of $T_<$ states.

Nuclues	J^π	$\bar{E}(T_<)$ (MeV)	$E(T_>)$ (MeV)	ΔE_s (MeV)	$\frac{\Delta V}{\Delta B}$	V_1 (MeV)
^{27}Al	$5/2^+$	1.06	8.55	7.5	1.66	216
	$1/2^+$	1.10	6.82	5.7	1.97	195
	$3/2^+$	2.88	7.75	4.9	1.86	158
	$7/2^-$	6.58	10.50	3.9	1.76	119
^{31}P	$1/2^+$	0.70	7.16	6.5	1.93	251
	$3/2^+$	1.58	6.41	4.8	1.82	175
	$7/2^-$	4.43	9.54	5.1	1.69	172
^{35}Cl	$3/2^+$	0.00	5.66	5.7	1.78	230
	$7/2^-$	3.16	7.54	4.4	1.62	162
	$3/2^-$	4.13	7.84	3.7	2.15	180

TABLE VII. Coulomb energy differences for ^{27}Mg–^{27}Al.

States in ^{27}Mg		Analogs in ^{27}Al		
E_x (keV)	J^π	E_x (keV)	J^π	ΔE_C (keV)
0	$1/2^+$	6815	$1/2^+$	4980
982	$3/2^+$	7750	$3/2^+$	4953
1692	$5/2^+$	8550	$5/2^+$	5023
3470	$1/2^+$	10 216	$3/2^-$	4831
3550	$3/2^-$	10 240	$1/2^+$	4935
3757	$7/2^-$	10 500	$7/2^-$	4908

where $Q[^{27}\text{Mg}(p,n)]$ was taken to be 1835 keV and $Q[^{31}\text{Si}(p,n)]$ was taken to be 694 keV. The average value of ΔE_C for ^{27}Al is 4938 keV and that for ^{31}P is 5666 keV.

For a nucleus of charge Z and radius R the Coulomb energy as given by Swamy and Green[24] is

$$E_C = \tfrac{3}{5} e^2 \frac{Z^2}{R}\left(1 - \frac{C}{Z^{2/3}}\right),$$

where $C = 764$ keV for $Z > 10$. The Coulomb energy difference between nuclei of charges $Z+1$ and Z is given[25] to a good approximation by

$$\Delta E_C = \tfrac{3}{5}\frac{e^2}{R}\left[(2Z+1) - \tfrac{4}{3}C(Z+\tfrac{1}{2})^{1/3}\right].$$

We can solve this equation for the charge radius R and compare with the results of Anderson, Wong, and McClure,[26] who were able to use $1.27A^{1/3}$ fm up to Nb. We obtain $1.320A^{1/3}$ fm for ^{27}Mg-^{27}Al and $1.287A^{1/3}$ fm for ^{31}Si-^{31}P.

The radius parameter for the mass-27 systems is approximately 0.03 fm larger than the one for the mass-31 systems. The difference represents about 110 keV in the Coulomb energy difference for ^{27}Mg-^{27}Al. If this difference were to be ascribed to the influence of deformation on the Coulomb energy

TABLE VIII. Coulomb energy differences for ^{31}Si–^{31}P.

States in ^{31}Si		Analogs in ^{31}P		
E_x (keV)	J^π	E_x (keV)	J^π	ΔE_C (keV)
0	$3/2^+$	6410	$3/2^+$	5716
750	$1/2^+$	7150	$1/2^+$	5706
1687	$(3/2,5/2)^+$	a		
2310	$3/2^+$	a		
2782	$5/2^+$	a		
3130	$(7/2)^-$	9400	$7/2^-$	5576

[a] Not seen.

shift given by [27]

$$\Delta E_C(\delta) \approx (1 - \tfrac{4}{45}\delta^2)\Delta E_C(0),$$

the value for δ would be 0.5.

SUMMARY

We have measured 26 angular distributions for the reaction ^{26}Mg(^{3}He, d)^{27}Al for transitions ranging from the ground state to 10.50-MeV excitation, and 18 angular distributions for the reaction ^{30}Si(^{3}He, d)^{31}P for transitions from the ground state to 9.40-MeV excitation. The experimental data were subjected to a DWBA analysis; the resulting theoretical curves agree well with the experimental data. Spectroscopic factors were deduced from the fits to the experimental data and compared with the results of experiments made at lower bombarding energy. Agreement was satisfactory, with the present experiment deducing somewhat less strength for the ground-state transitions. Core-polarization can explain, at least qualitatively, the fragmenting of the $T_<$ states and some features of the proton-stripping strengths to ^{27}Al and ^{31}P. The value of the isovector potential was determined for several orbits from the splitting of the analog state and the centroid of the $T_<$ states. The average value for V_1 is about 189 MeV. Finally, charge radii were calculated for Coulomb energy differences; ^{27}Al requires a larger radius parameter than ^{31}P.

---

†Work performed under the auspices of the U. S. Atomic Energy Commission.

[1]W. Bohne, H. Fuchs, K. Grubisch, M. Hagen, H. Homeyer, V. Janetzki, H. Lettan, K. H. Maier, H. Morgenstern, P. Pietrzyk, G. Roschert, and J. A. Scheer, Nucl. Phys. A131, 273 (1969).

[2]W P. Alford, D. Cline, H. E. Gove, K. H. Purser, and S. Skorka, Nucl. Phys. A130, 119 (1969).

[3]M. Betigeri, R. Bock, H. H. Duhm, S. Martin, and R. Stock, Z. Naturforsch. 21a, 980 (1966).

[4]A. C. Wolff and H. G. Leighton, Nucl. Phys. A140, 319 (1970).

[5]B. Lawergren, Nucl. Phys. A90, 311 (1967).

[6]C. van der Leun, D. M. Sheppard, and P. M. Endt, Nucl. Phys. A100, 316 (1967).

[7]W. G. Davies, W. K. Dawson, and G. C. Neilson, Phys. Letters 19, 576 (1965).

[8]G. I. Harris, H. J. Hennecke, and F. W. Prosser, Jr., Phys. Letters 9, 324 (1964).

[9]F. S. Goulding, D. A. Landis, J. Cerny, and R. H. Pehl, Nucl. Instr. Methods 31, 1 (1964).

[10]P. M. Endt and C. van der Leun, Nucl. Phys. A105, 1 (1967).

[11]P. D. Kunz, private communication.

[12]R. W. Zurmuhle and C. M. Fou, Nucl. Phys. A129, 502 (1969).

[13]R. H. Bassel, Phys. Rev. 149, 791 (1966).

[14]J. B. French and M. H. Macfarlane, Nucl. Phys. 26, 168 (1961).

[15]D. Robson, Phys. Rev. 137, 535 (1965).

[16]J. B. French, Argonne National Laboratory Report No. ANL-6878, 1964 (unpublished), p. 181.

[17]A. M. Lane, Nucl. Phys. 35, 676 (1962).

[18]A. Graue, L. H. Herland, J. R. Lien, G. E. Sandvik, E. R. Cosman, and W. H. Moore, Nucl. Phys. A136, 577 (1969).

[19]G. Vourvopoulos and J. D. Fox, Phys. Rev. 177, 1558 (1969).

[20]G. Vourvopoulos, J. D. Fox, and B. Rosner, Phys. Rev. 177, 1789 (1969).

[21]L. V. Krasnov, V. F. Litvin, and V. D. Lyntin, Yadern. Fiz. 9, 40 (1969) [transl.: Soviet J. Nucl. Phys. 9, 24 (1969)].

[22]G. R. Satchler, R. M. Drisko, and R. H. Bassel, Phys. Rev. 136, B637 (1964).

[23]P. C. Sood, Nucl. Phys. 89, 535 (1966).

[24]N. V. J. Swamy and A. E. S. Green, Phys. Rev. 112, 1719 (1958).

[25]C. J. Batty, R. S. Gilmore, and G. H. Stafford, Nucl. Phys. 75, 599 (1966).

[26]J. D. Anderson, C. Wong, and J. W. McClure, Phys. Rev. 129, 2718 (1963).

[27]M. H. Macfarlane, in *Isobaric Spin in Nuclear Physics*, edited by J. D. Fox and D. Robson (Academic Press Inc., New York, 1966), p. 399.